AWES

15th Australasian Wind Engineering Society Workshop

23-24 February 2012 - Sydney Australia
the University of Sydney

Workshop Proceedings

Australian Government
Geoscience Australia

THE UNIVERSITY OF SYDNEY

TaylorThomsonWhitting

leap australia pty ltd

Kenelec Scientific

ARUP

Workshop Program and Table of Contents

* This paper was not peer-reviewed.

1230 - 1330	Lunch	
1330 - 1445	**Session 7 – Structural dynamics** ***Chair: Dr Mick Chay***	
1330 - 1345	Evaluation of HFBB analysis under the effects of surrounding buildings *K. Tse and K. Wong*	129
1345 - 1400	Estimation of torsional loads on tall buildings *A. Rofail and N. Truong*	133
1400 - 1415	Bifurcation prediction of the aeroelastic galloping model with structural and damping non-linearities *G. Vio*	137
1415 - 1430	Wind loads on extension of light towers at AAMI Stadium Adelaide *N. Mackenzie, J. Holmes, G. Rowland and J. Gaekwad*	141
1430 - 1445	**Close**	
1445 - 1600	AWES research priorities forum	

15th Australasian Wind Engineering Society (AWES) Workshop
Sydney, Australia
23-24 February, 2012

Vortex formation above prismatic-shaped cliffs; an experimental and numerical investigation

S. Cochard[1], A. Montlaur[2], D. F. Fletcher[1], C. W. Letchford[3] and T. A. Earl[1]

[1]Faculty of Engineering and IT
The University of Sydney, Sydney, NSW 2006, Australia

[2]Escola d´Enginyeria de Telecomunicació i Aeroespacial de Castelldefels
Universitat Politècnica de Catalunya, Castelldefels, Spain

[3]Department of Civil & Environmental Engineering
Rensselaer Polytechnic Institute, Troy, NY, USA

Abstract

Computational Fluid Dynamics (CFD) simulations and Particle Image Velocimetry (PIV) measurements are used to study the flow over a cliff of isosceles prismatic elements arranged in sawtooth patterns at a yaw angle of 0°. The CFD and the PIV give similar results; as the flow approaches the cliffs, it accelerates and moves up to pass the obstruction and generates two delta wing vortices on the top surface of the cliff.

Introduction

Wind Energy is one of the fastest growing sources of renewable energy, adding 24% to its installed capacity in 2009 to reach 159GW worldwide (WWEA, 2010). Typically taking advantage of speed-up effects over topography, coastal and exposed hilltops are preferred development sites. In Texas, which became the highest installed wind energy capacity state in the US in 2008, escarpment sites were commonly being developed, while on the south coast of Australia, many exposed headlands were seen as potentially the best sites for wind farms. In a recent review, Ayotte (2010) indicated that such sites can generate substantial turbulence, particularly lateral turbulence that is damaging to wind turbines and can seriously impact wind energy forecasts.

The present study was motivated to develop a better understanding of the flow generated over complex topography as a first step in developing better site classifications, using wind-tunnel tests and numerical simulations. Whereas the flow over a forward facing step (a 2-dimensional cliff) has been well studied (Sherry et al, 2010), the study of steep 3-dimensional topography, such as found on inland escarpments and coastal headlands has received very little attention. The work of Glanville and Kwok (1997) is one of the few experimental studies of steep topography that was linked to a specific full scale site where limited field measurements were undertaken. However, the mountain studied there was nominally 2-dimensional.

In the present study, first a series of wind-tunnel tests of generic 3-dimensional topography utilising isosceles triangular elements arranged in sawtooth patterns were performed, and second, Computational Fluid Dynamics (CFD) simulations were studied to develop better understanding of flow complexity over such surface level changes with shape and wind direction.

Methods

Wind-Tunnel Tests

Figure 1 presents a sketch of the 2.5 m wide cliff model installed in the boundary layer wind tunnel of the School of Civil Engineering at the University of Sydney. The tunnel is an open circuit wind tunnel with a test section of 2.0 × 2.5 m and a fetch of 20 meters. The fetch can be equipped with variable levels of roughness to produce different boundary layer profiles with specific turbulence characteristics. The maximum wind speed in the boundary layer section is of the order of 16 m/s. A relatively rough 1:400 scale atmospheric boundary layer simulation was developed using a trip-board, 4 spires and carpet roughness.

The cliff face was composed of right-angled isosceles triangular prisms, referred to as 'triangles' hereafter. The model was made from high-density polystyrene and all the triangular prisms had a base length of 500 mm and a height of 100 mm. The middle triangle was made from plywood. The three components of the velocity were measured in three horizontal planes over the plywood cliff using a stereo-PIV system (David and Gicquel, 2006; Felli et al, 2002; Prasad, 2000). The turntable with the attached model was rotated to simulate different incoming flow angles. In Figure 1, the flow is moving from left to right, the yaw angle of the cliff is 0°, and the coordinate system *xyz* is fixed relative to the tunnel, with its zero at the centre of rotation of the turntable. In this paper, by convention, the stream-wise direction is along the *x*-axis and the upstream free flow does not have any mean component along the *y* or *z*-axes.

The stereo-PIV system, used to measure the three components of the velocity, was composed of a double head 200 mJ-per-pulse laser and two 11 MPx cameras. It was set up, in this case, to measure the velocity on a plane of 0.3 × 0.2 m. For each test, 60 PIV velocity fields were recorded and averaged to compute the mean flow and the turbulence intensity.

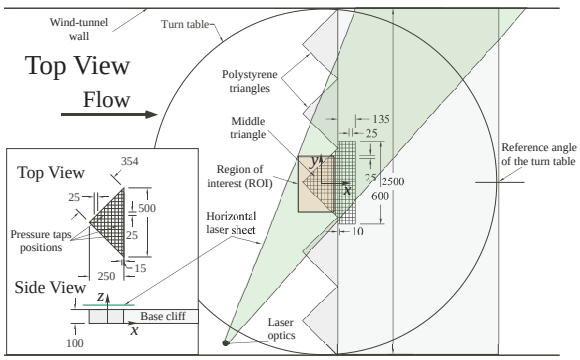

Figure 1: Sketch of the configurations of the cliff model with the positions of the PIV window.

The 5-triangle cliff spanned the full 2.5 m width of the wind tunnel and was 4.7 m long with an additional 0.9 m long downstream wedge. The three components of the velocity were mea-

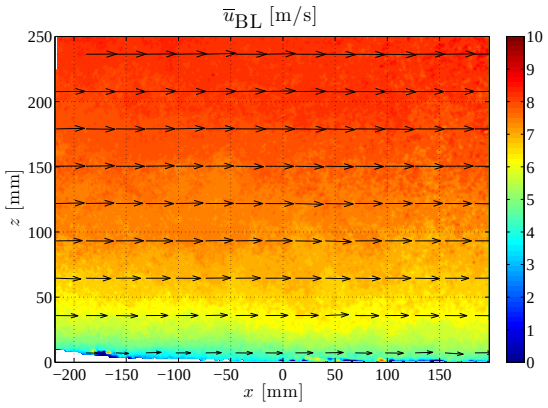

Figure 2: Stream-wise velocity u, in the xz-plane, of the boundary layer without any obstacle.

sured over the middle prismatic cliff, at three different heights above the cliff, for 9 different incoming flow angles. While the measuring plane was set at 14.3 mm above the cliff, three incoming flow speeds ($u_{\max}$ of 7, 9 and 12 m/s) were tested for each angle to ensure that the results were independent of the incoming flow velocity. For all other tests the velocity was constant (9 m/s). In this paper, only the PIV results at 14.3 mm above the cliff, with 0° yaw angle, and a $u_{\max}$ of 9 m/s are presented.

The PIV system was also set to measure the boundary layer profile in a vertical plane without any obstruction (Figure 2).

Numerical Simulations

The flow being modelled is a steady flow, with a Reynolds number of approximately 100,000 based on the length of the triangular cliff and on the inlet velocity at the height of the cliff. The fluid is air, considered incompressible and isothermal, at a temperature of 25°C. The computational domain is shown in Figure 3 and is 10 l_{cliff} long (3 l_{cliff} in front of the cliff) and 10 h_{cliff} high, based on a cliff length (l_{cliff}) of 0.25 m and a cliff height (h_{cliff}) of 0.1 m. The zone of interest of this simulation is a rectangle located at $z = 0.1143$ m above the cliff and going for 0.2 m along the cliff, that is $-0.1\ \mathrm{m} < x < 0.1\ \mathrm{m}$ and $-0.15\ \mathrm{m} < y < 0.15\ \mathrm{m}$. This zone is where PIV data are available.

The following boundary conditions were set for the numerical

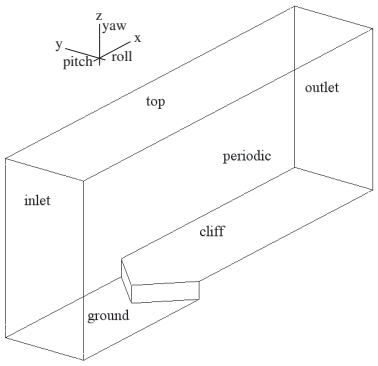

Figure 3: Computational domain.

simulations. A horizontal velocity boundary layer profile of $u_{\mathrm{BL}} = 1.14 \cdot \ln(6119z + 1)$ in [m/s], where z is the height in meters, a turbulence intensity of 0.17, corresponding to the experimental data, and an eddy viscosity ratio of 10 were set at the inlet. The top boundary was also set as an inlet with the same properties as the real inlet. An average static pressure of 0 Pa was set at the outlet. The two lateral sides of the parallelepiped were set as periodic boundaries (so only one triangular cliff was simulated). The cliff ground was treated as a no-slip smooth wall, whereas the ground upstream of the cliff was considered as a rough wall with a sand-grain roughness of 0.015 m corresponding to a physical roughness of around 0.5 mm.

All numerical simulations were carried out with the commercial CFD solver, ANSYS CFX13 (ANSYS 2010). CFX13 is based on a coupled finite volume solver for the mass and momentum (and energy if required) equations. The numerical scheme uses a collocated pressure based method and a modified Rhie-Chow algorithm to avoid decoupling. The resulting algebraic equations are solved by an algebraic multi-grid method. All velocity calculations use a second order bounded differencing scheme while a first order upwind scheme is implemented for the convective terms in the turbulence equations, and a second order scheme is used for all diffusive terms.

The SST (Shear Stress Transport) model is used in this work. It combines the $k-\varepsilon$ and the $k-\omega$ models by way of a blending function Menter (1994). The blending function ensures that the $k-\varepsilon$ model is used in the free shear region, while the $k-\omega$ model is used near walls so the flow is resolved through the viscous sublayer. The SST model was designed to give highly accurate predictions of the onset and the amount of flow separation under adverse pressure gradients by the inclusion of transport effects into the formulation of the eddy-viscosity ANSYS (2010). This results in a major improvement in terms of flow separation predictions. The superior performance of this model has been demonstrated in a large number of validation studies Bardina et al (1997). The curvature correction option was activated.

The computational mesh was composed of 1.3 million tetrahedral elements. An inflation mesh comprising 30 layers was used along the ground in front of and on top of the cliff, with a first layer thickness of 0.1 mm. A body-sizing of 4 mm was used in the region of interest, whereas a coarser body sizing of 20 mm was used around the cliff. Within the computational mesh, the coarsest size of element was set to 70 mm. A mesh dependency was performed and it corroborated the choice of the mesh used in this study.

Two convergence criteria were set. First, the root mean square residuals were set to be below 10^{-4}. Second, three monitor points were created at the height of interest $z = 0.1143$ m, one centred at the beginning of the cliff and two others further away along the cliff edge. The calculation was stopped when values of velocity and pressure at these points did not change anymore.

Results

Delta wing vortex

The flow over the triangular shaped cliffs is similar to the flow over a delta wing, (Johari and Moreira, 1998). As the flow approaches the cliffs, it accelerates and moves up to pass the obstruction. The streamlines in Figure 5 show the formation of the vortices over the cliff, while Figure 4 compares quantitatively the results obtained with the PIV and the CFD simulations.

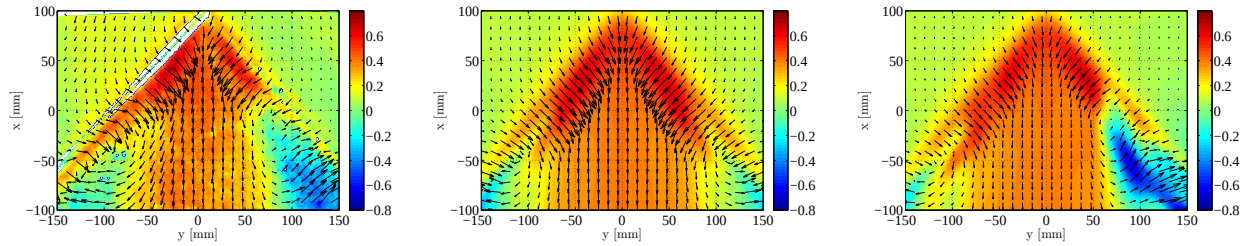

(a) PIV measured M_u (b) CFD computed M_u; ideal case (c) CFD computed M_u; inclined cliff

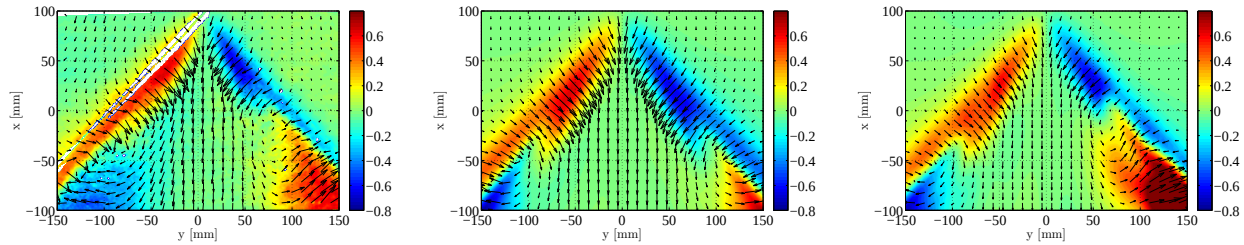

(d) PIV measured M_v (e) CFD computed M_v; ideal case (f) CFD computed M_v; inclined cliff

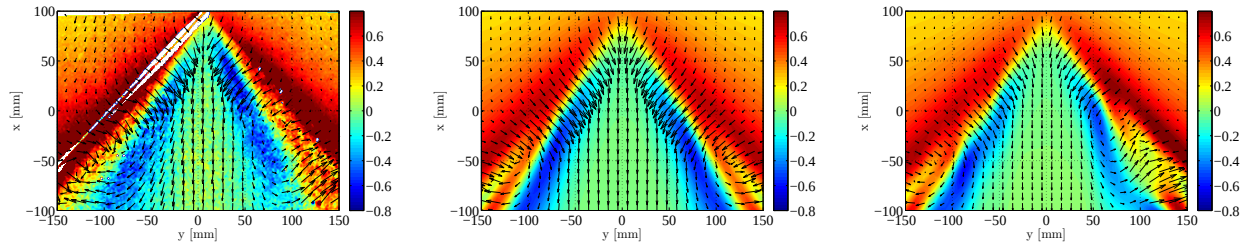

(g) PIV measured M_w (h) CFD computed M_w; ideal case (i) CFD computed M_w; inclined cliff

Figure 4: Speed-up ratio $\mathbf{M} = (M_u, M_v, M_w)$ at $z = 14.3$ mm over the cliff. The first column ((a), (d) and (g)) represent the PIV results, the second column ((b), (e) and (h)), the CFD results for an ideal case and the third column ((c), (f) and (i)), the CFD results for an inclined cliff with a 1° roll angle and a 1° pitch angle.

Speed-up ratio

All velocities presented in the following sections were normalized using the speed-up ratio $\mathbf{M}(z = h)$, computed as follows for a given height h:

$$\mathbf{M}(z=h) = \frac{\overline{\mathbf{V}}_{\text{cliff}}(z = h + h_{\text{cliff}}) - \overline{\mathbf{V}}_{\text{BL}}(z=h)}{|\overline{\mathbf{V}}_{\text{BL}}(z=h)|} \quad (1)$$

where $\overline{\mathbf{V}}_{\text{cliff}}$ is the mean velocity measured at a height h above the cliff, h_{cliff} is the height of the cliff, and, $\overline{\mathbf{V}}_{\text{BL}}$ is the mean velocity of the boundary layer measured at a height h above the wind tunnel floor without the cliff model. To simplify the notation, the over-line above $\mathbf{M}$ was dropped even though the speed-up ratio is defined as the mean value. A speed-up ratio of 1 represents an increase of velocity by a factor 2 over the cliff, a speed-up ratio of 0 denotes no change in velocity and a speed up ratio of -1 indicates a stagnation point with a velocity of zero over the cliff.

Comparison of CFD and experimental data

Figure 4 compares the three components of the speed-up ratio $\mathbf{M} = (M_u, M_v, M_w)$ at $z = 14.3$ mm obtained from the PIV measurements (first column, Figures 4a, 4d and 4g) and two CFD simulations (second and third columns, Figures 4b, 4e, 4h, 4c, 4f and 4i). The middle column of Figure 4 represents the CFD results for an ideal case, where the cliff is horizontal and parallel to the floor. The speed-up results, in this case, are symmetric over the triangle:

- A speed-up ratio M_u (Figure 4b) between 0.3 and 0.5

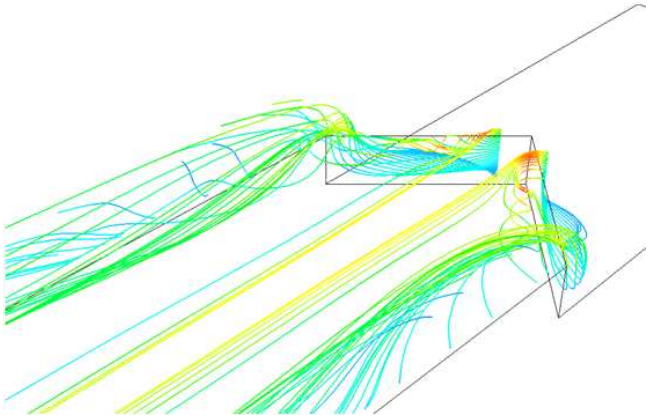

Figure 5: Velocity streamlines around the cliff for an incoming flow of 0°.

along the symmety axis of the triangle demonstrates an increase of the stream-wise velocity of 30 to 50% and could, a priori, justify the installation of wind turbines on the top of the cliff. As the power of a wind turbine is a function of the velocity to the power of 3, the substantial power gain from a speed-up ratio of 0.4 is 2.7. Away from the axis of symmetry of the triangle, the speed-up ratio can have negative values down to -0.5, which means that the stream-wise velocity above the cliff is half the velocity of the free stream at the same relative height h. Clearly these are not good positions for a wind turbine as the power output is significantly reduced.

- M_w (Figure 4h) clearly shows an upward flow upstream of the cliff with a maximum upward velocity at the cliff edge. Once the wind has passed the edge, the two vortices start to form and grow in a cone of 30°.
- M_v (Figure 4e) displays the growth of the vortex cone both in the vertical and horizontal axis. Close to the tip of the triangle, the 14.3-mm high measurement plane only records an inward M_v flow; the measurement plane is at the top edge of the vortices. Closer to the downstream end of the triangle, M_v is of opposite sign, indicating an outward flow (from the centre of the triangle to the edge); the measurement plane is in the lower part of the vortices.

A wind turbine positioned in one of these vortices would face not only a large velocity gradient, as the amplitude and direction of the incoming flow vary, but also a strong level of turbulence.

The PIV results, contrary to the ideal CFD case, show non-symmetric results; the vortex on the right side of the triangle is larger than the one on the left. The asymmetry is particularly visible on Figure 4d; the centre of rotation of the windward vortex crosses the measurement plane about 20 mm upstream of the leeward vortex centre of rotation. Once the vortex centre of rotation crosses the measurement plan, the component v of the velocity changes direction from inward (toward the centre of the triangle) to outward (toward the edge of the triangle).

The turntable, on which the model of the cliff is fixed , was not sufficiently rigid and had a small ($< 1°$) roll and pitch angle. The third column of Figure 4 shows the results of the CFD simulations with the triangular cliff inclined with a 1° roll angle and a 1° pitch angle. These results are consistent both qualitatively and quantitatively with the PIV results. The shape of the vortices was found to be more sensitive to the roll and pitch angle than to the yaw angle. When the cliff is not sitting perfectly horizontal, one side of the triangle is showing a higher cliff surface (right side) than the other one (left side) and, as a result, creates a larger vortex.

Discussion

Both the CFD simulations and the wind tunnel tests give, as anticipated, similar results. The PIV measurements over the cliff presented non-symmetric results, which could not be interpreted before the CFD simulations were carried on. The CFD simulation highlighted the sensitivity of vortex formation to the roll and pitch angles. With a pitch and roll angle of 1° the CFD simulations are in good agreement with the PIV results. After investigating the experimental setup, it was confirmed, that, once the cliff model is in place, the turntable had a 1° roll and pitch angle.

Conclusion

When an atmospheric boundary layer flow passes over generic triangular-shape cliffs, two delta-wing vortices are created on each cliff. These vortices are strong and turbulent and quite sensitive to the pitch and roll angles. The speed-up ratio over a triangular cliff with a yaw angle of 0° ranges from -0.8 to 0.8, i.e, from a velocity that is only 20% of the free stream velocity to a velocity of 180%. The complexity of the flow field has been revealed in this unique three-dimensional study and makes this a difficult region for taking full advantage of potential speedup effects associated with cliffs for wind energy considerations. The CFD results, combined with the PIV measurements, proved to be very valuable to fully understand the flow over the cliff and can be an essential tool to position the wind-turbine.

*

References

ANSYS (2010) CFX users manual. URL www.ansys.com

Ayotte K (2010) Physical and computational modelling of topographically generated wake turbulence. In: Cechet B (ed) 14th Australasian Wind Engineering Society Workshop, AWES, Geoscience Australia

Bardina J, Huang P, Coakley T (1997) Turbulence modeling validation testing and development. NASA Technical Memorandum 110446

David L, Gicquel P (2006) Evolutions de la technique PIV à travers quelques conférences internationales de 2000 à aujourd'hui. In: Congrès Francophone de Techniques Laser, CFTL, Toulouse, France

Felli M, Pereira F, Calcagno G, Felice FD (2002) Application of stereo-PIV: Propeller wake analysis in a large circulating water channel. In: 11th Int. Symp. on Applications of Laser Techniques to Fluid Mechanics, Lisbon, Portugal

Glanville MJ, Kwok KCS (1997) Measurements of topographic multipliers and flow separation from a steep escarpment, part II: Model-scale measurements. Journal of Wind Engineering and Industrial Aerodynamics 69-71:893–902

Johari H, Moreira J (1998) Direct measurement of delta-wing vortex circulation. AIAA Journal 36(12):2195–2203

Menter F (1994) Two-equation eddy-viscosity turbulence models for engineering applications. AIAA Journal 32(8):1598–1605

Prasad AK (2000) Stereoscopic particle image velocimetry. Experiments in Fluids 29(2):103–116

Sherry M, Lo Jacono D, Sheridan J (2010) An experimental investigation of the recirculation zone formed downstream of a forward facing step. Journal of Wind Engineering and Industrial Aerodynamics 98(12):888–894

WWEA (2010) World Wind Energy Report. World Wind Energy Association